

Using Green's Functions to Initialize and Adjust a Global, Eddying Ocean Biogeochemistry General Circulation Model

H. Brix^{a,*}, D. Menemenlis^b, C. Hill^c, S. Dutkiewicz^c, O. Jahn^c, D. Wang^c,
K. Bowman^b, H. Zhang^d

^a*Department of Atmospheric and Oceanic Sciences, The University of California, Los Angeles, CA, USA. Tel: +1-310-825-4526; fax: +1-310-206-3051*

^b*California Institute of Technology, Jet Propulsion Laboratory, Pasadena, CA, USA*

^c*Massachusetts Institute of Technology, Cambridge, MA, USA*

^d*Joint Institute for Regional Earth System Science and Engineering, The University of California, Los Angeles, CA, USA*

Abstract

Fluxes between carbon reservoirs on Earth are central for understanding the global carbon cycle. The goal of the NASA Carbon Monitoring System (CMS) Flux Pilot Project is to utilize the full suite of NASA data, models, and assimilation capabilities for attributing changes in the atmospheric accumulation of carbon dioxide to spatially resolved fluxes. For the oceanic part of this project, we introduce “ECCO2-Darwin”, a new ocean biogeochemistry general circulation model based on combining the following pre-existing components: (i) a full-depth, eddying, global-ocean configuration of the Massachusetts Institute of Technology general circulation model (MITgcm), (ii) an adjoint-method-based estimate of ocean circulation from the Estimating the Circulation and Climate of the Ocean, Phase II (ECCO2) project, (iii) the MIT ecosystem model “Darwin”, and (iv) a marine carbon chemistry model. Initializing a global, eddying biogeochemical ocean general circulation model like ECCO2-Darwin poses major challenges due to computational constraints and to model drifts. Here, we present a proof-of-concept study that applies a Green's functions approach to optimize modeled air-sea CO₂ fluxes by adjusting initial conditions and air-sea gas exchange coeffi-

*Corresponding author

Email address: hbrix@ucla.edu (H. Brix)

cients. We use observations of carbon dioxide partial pressure ($p\text{CO}_2$) for 2009–2010, global air-sea CO_2 flux estimates, and the seasonal cycle of the Takahashi et al. (2009) climatology to constrain the model and to obtain initial fields of dissolved inorganic carbon, alkalinity, and oxygen that allow us to improve estimates of air-sea carbon fluxes at high spatial and temporal resolution. We have performed a variety of sensitivity experiments starting from different initial conditions, as well as experiments that perturb air-sea gas exchange parameters and the ratio of particulate inorganic to organic carbon. The Green’s functions approach yields a linear combination of these sensitivity experiments, which minimizes the model-data differences; it is a first step towards a more realistic representation of the ocean carbon cycle by the ECCO2-Darwin model. Comparisons with observations help identify critical regions for improvement, for instance, regions of overly strong carbon uptake in the Southern Ocean and weak outgassing the Equatorial Pacific.

Keywords:

Carbon Monitoring System, ocean biogeochemical circulation model, Green’s function, data assimilation

1. Introduction

The components of the global carbon cycle interact through fluxes between the carbon reservoirs on our planet: atmosphere, land, oceans, and the geosphere. Understanding the exchange processes between these reservoirs requires knowledge about these fluxes. As there is no global scale observation network in place that could provide these flux estimates, we need to combine existing observations with models to compute them indirectly. To achieve the most realistic results, models can be constrained by observational data, especially global space-based observations that provide information about the physical and biological state of the land, atmosphere or ocean.

The goal of the NASA Carbon Monitoring System (CMS) Flux Pilot Project is to incorporate the full suite of NASA data, models, and assimilation capabilities to attribute changes in the atmospheric accumulation of carbon dioxide to spatially resolved fluxes¹. The oceanic component of these fluxes is of critical importance as it is estimated that the oceans have absorbed $48 \pm 9\%$ of the anthropogenic CO_2 emitted during 1880–1994, that is,

¹compare <http://carbon.nasa.gov> and <http://cmsflux.jpl.nasa.gov/>

17 since the beginning of the industrial period (Sabine et al., 2004). The current
18 oceanic CO₂ uptake is estimated to about a quarter of the anthropogenic
19 emissions (Le Quéré et al., 2010). The ECCO2-Darwin model, described
20 herein, along with the NASA Ocean Biogeochemical Model (NOBM; Gregg
21 and Casey, 2007), provides spatially resolved oceanic CO₂ fluxes constrained
22 by observations of the physical ocean and ship-based CO₂ measurements
23 for the CMS project. These fluxes are calculated for the period 2009–2010,
24 the time frame for which GOSAT (Kuze et al., 2009) atmospheric $x\text{CO}_2$ (dry
25 mole air fraction of CO₂) measurements are available. The ocean fluxes serve
26 as a priori surface forcing for the “top-down” atmospheric flux estimates in
27 the CMS project.

28 Although the flux of CO₂ across the air-sea interface cannot be measured
29 directly, its magnitude is known to depend on the difference ($\Delta p\text{CO}_2$) be-
30 tween the partial pressures of CO₂ of the ocean ($p\text{CO}_2$) and of the atmosphere
31 ($p\text{CO}_2^{\text{atm}}$). The air-sea CO₂ flux for a given $\Delta p\text{CO}_2$ is usually estimated us-
32 ing a parameterization where the gas exchange coefficients depend on wind
33 speed at the surface of the ocean (e.g., Wanninkhof, 1992; Takahashi et al.,
34 2002; Sarmiento and Gruber, 2006).

35 Oceanic $p\text{CO}_2$ depends on temperature and on other components of the
36 oceanic carbon system, which in turn depend on ocean circulation and bio-
37 logical activity. Observations of $p\text{CO}_2$ are based on in-situ measurements and
38 have been compiled into large data bases (Takahashi et al., 2002, 2009; Pfeil
39 et al., 2012). Takahashi et al. (2002) used 940,000 measurements of surface-
40 water $p\text{CO}_2$ obtained since the International Geophysical Year of 1956–1959
41 to compile a gridded climatological monthly distribution of surface $p\text{CO}_2$ for
42 the reference year 1995, later updated for the year 2000 (Takahashi et al.,
43 2009).

44 On the basis of the available measurements numerous efforts have been
45 undertaken to quantify the oceanic uptake of CO₂ and its spatial structure
46 (e.g., Keeling et al., 1996; Battle et al., 2000; Takahashi et al., 2002, 2009),
47 its temporal variability, and the magnitude of its anthropogenic component
48 (e.g., Gloor et al., 2003; McNeil et al., 2003; Sabine et al., 2004).

49 Other approaches to quantify air-sea CO₂ fluxes are based on atmospheric
50 CO₂ mixing ratios (e.g., Conway et al., 1994, and many others) and transport
51 inversions (e.g., Bousquet et al., 2000; Gurney et al., 2002; Rödenbeck et al.,
52 2003; Baker et al., 2006), which “estimate the regional distribution of air-
53 surface CO₂ fluxes using the spatiotemporal variability in atmospheric CO₂
54 concentration measurements” (Le Quéré et al., 2009). With regard to the

55 oceans the results of these studies are difficult to interpret as the oceanic
56 signal variability is small compared to terrestrial fluxes. Nevertheless, they
57 provide estimates independent from gas exchange parameterizations.

58 Another air-sea-CO₂-flux estimation method that does not require knowl-
59 edge of a gas exchange coefficient is based on inverse calculations of oceanic
60 transports using ocean-interior data of dissolved inorganic carbon (*DIC*) and
61 on ocean circulation models (Gloor et al., 2003; Mikaloff Fletcher et al., 2006,
62 2007; Gruber et al., 2009). While this method allows a certain (coarse) re-
63 gionalization of model results, it only yields long-term CO₂ fluxes without
64 temporal variability.

65 Numerous biogeochemical ocean forward models have been developed
66 (Aumont and Bopp, 2006; Le Quéré et al., 2007; Thomas et al., 2008; Doney
67 et al., 2009; Buitenhuis et al., 2010; Assmann et al., 2010; Galbraith et al.,
68 2010, to name a few recent ones). These models differ substantially in resolu-
69 tion as well as in the formulation of model physics, biology, and the compo-
70 nents of the carbon cycle, depending on the questions they intend to answer.
71 In light of societal interest in anthropogenic changes of carbon sources and
72 sinks, substantial effort went into improving these models to address recent
73 changes of oceanic carbon uptake (e.g., Le Quéré et al., 2007, 2009, 2010;
74 Lenton et al., 2012) and possible future development and feedback under
75 climate change scenarios (e.g., Roy et al., 2011; Séférian et al., 2012).

76 For the specific task of developing a Carbon Monitoring System, the re-
77 quirement of an ocean component that represents the current state of the
78 oceans as realistically as possible leads to following two criteria. First, to cap-
79 ture the fine scale structure of sources and sinks and their temporal changes
80 in certain regions it is desirable to have a resolution that is at least eddy-
81 permitting. The North Atlantic is an example for a region exhibiting such
82 high variability on both temporal and spatial scales (compare, for instance,
83 Fig. 3 in Le Quéré et al., 2009). Second, observational data should be incor-
84 porated into the model simulations to the highest degree possible. In order to
85 address these two requirements, we developed the ECCO2-Darwin model (as
86 described later in this paper), which combines eddy horizontal resolution
87 with state-of-the-art biogeochemistry and data assimilation capability.

88 When setting up an Ocean Biogeochemistry General Circulation Model
89 (OBGCM) with this type of specifications, one of the most difficult tasks
90 is to account for complications resulting from high computational cost. In
91 the ocean, where circulation is slow compared to the atmosphere, it can
92 take thousands of (model) years to reach an equilibrium state. As increased

93 spatial resolution requires more computing time, going to higher and higher
94 resolution diminishes the ability to spin-up models for a sufficiently long
95 time. Adding complexity to models by, for instance, including biogeochemical
96 cycles with many tracers, exacerbates the problem, as the model equations
97 have to be solved for each additional tracer.

98 Another problem associated with long spin-ups is model drift, that is,
99 the increasing biases between the model simulation and nature. Although
100 initial conditions are traditionally chosen to be as close to nature as possible,
101 systematic model or boundary condition errors will cause the simulation to
102 drift from a state near the attractor of nature to a state close to the attractor
103 of the model (Toth and Peña, 2007). If this model equilibrium state is too
104 far from nature, estimates of air-sea fluxes and the underlying physics and
105 biogeochemistry that drive these fluxes will be unrealistic, that is, they will
106 not or only imperfectly represent the natural phenomena they supposed to
107 model.

108 For short model integrations that circumvent these drift issues and allow
109 high resolution and model complexity, choosing initial conditions becomes
110 a critical issue. The availability of oceanic data at any given point in time
111 chosen to be the models starting point is extremely limited. While remote
112 sensing has improved the data situation drastically, it only supplies data for
113 the top layer of the ocean and gives very little information that can be used
114 to initialize ocean biogeochemistry.

115 To solve this initialization problem for all biogeochemical quantities simul-
116 taneously and to avoid producing unrealistic air-sea carbon flux estimates,
117 we use a simple, physically-consistent data assimilation approach based on
118 model Green's functions, that is, on forward model sensitivity experiments
119 (Menemenlis et al., 2005a). The advantages of this method are simplicity
120 of implementation, the possibility of obtaining complete a posteriori error
121 statistics for the parameters being estimated, and improved robustness in
122 the presence of nonlinearities. One of the trade-offs associated with this
123 method is that computational cost increases linearly with the number of
124 control parameters (Menemenlis et al., 2005a).

125 This study is meant to (i) introduce the ECCO2-Darwin OBGCM, (ii)
126 be a proof-of-concept for the application of Green's functions to the prob-
127 lem of initializing high resolution biogeochemical models, and (iii) describe
128 some residual problems of the ECCO2-Darwin estimates that need to be
129 addressed in future work. We start by introducing the various components
130 of the ECCO2-Darwin OBGCM (Section 2). We then describe the initial

131 model simulation (Section 3) and give details about the various sensitivity
132 experiments (Section 4). Next we describe the observations used to evaluate
133 and adjust the model solution (Section 5). In Sections 6 and 7, we describe
134 the data assimilation method and the optimized model realization. Finally
135 we evaluate this optimized solution and discuss residual errors in Section 8.

136 2. The ECCO2-Darwin Model

137 The ECCO2-Darwin Ocean Biogeochemistry General Circulation Model
138 is based on a global, eddy, ocean and sea ice configuration of the Mas-
139 sachusetts Institute of Technology general circulation model (MITgcm; Mar-
140 shall et al., 1997a,b) and on results from two separately funded projects: the
141 Estimating the Circulation and Climate of the Ocean, Phase II (ECCO2)
142 Project, which provides a data-constrained estimate of the time-evolving
143 physical ocean state, and the Darwin Project, which provides time-evolving
144 ocean ecosystem variables. Together, ECCO2 and Darwin, supplemented by
145 a carbon chemistry component, supply a time-evolving physical, biological,
146 and chemical simulation of oceanic carbon biogeochemistry. We developed
147 this new OBGCM in order to compute surface fluxes of carbon at high spatial
148 and temporal resolution for the NASA CMS Flux Pilot Project.

149 2.1. ECCO2

150 The ECCO2 global-ocean model configuration uses a cube-sphere grid
151 (Adcroft et al., 2004) with 18-km horizontal grid spacing and 50 vertical lev-
152 els (Menemenlis et al., 2005b, 2008). It includes a dynamic/thermodynamic
153 sea ice model (Losch et al., 2010; Heimbach et al., 2010). In a first step, the
154 ECCO2 model configuration was adjusted using a low-dimensional (Green’s
155 functions) estimation approach (Menemenlis et al., 2005a). In a second step,
156 the method of Lagrange multipliers, also known as the adjoint method (Wun-
157 sch and Heimbach, 2007), was used to adjust initial and time-evolving surface
158 boundary conditions. Data constraints for the adjoint-method optimization
159 include sea level anomaly from altimeters on Jason-1, Jason-2/Ocean Surface
160 Topography Mission (OSTM), and Environmental Satellite (Envisat); sea
161 surface temperature from the Advanced Microwave Scanning Radiometer-
162 EOS (AMSR-E); and temperature and salinity profiles from the Argo profil-
163 ing floats. The adjoint-method-based ECCO2 estimates of the global-ocean
164 circulation available at the beginning of this study were for year 2004 and

165 for 16 months starting in January 2009. These physical ocean circulation
166 estimates were used to drive the Darwin ecosystem model.

167 *2.2. Darwin and Ocean Chemistry*

168 The Darwin Project is an initiative to advance the development and ap-
169 plication of novel models of marine microbial communities, to identify the
170 relationships of individuals and communities to their environment, and to
171 connect cellular-scale processes to global microbial community structure (Fol-
172 lows et al., 2007; Follows and Dutkiewicz, 2011; Dutkiewicz et al., 2009). The
173 particular configuration used for the CMS Flux Pilot Project includes five
174 phytoplankton functional types (choices based on results from previous ver-
175 sions of the model, see Section 3.1) and two zooplankton types. The carbon
176 cycle is explicitly included in this configuration, along with those of nitrogen,
177 phosphorus, iron, silica, oxygen, and alkalinity. The carbonate chemistry fol-
178 lows the simplified model proposed by Follows et al. (2006) and air-sea CO₂
179 exchange is parameterized according to Wanninkhof (1992).

180 **3. VERSION 1: The First ECCO2-Darwin Simulation**

181 To obtain a first estimate of air-sea carbon fluxes for 2009 and 2010,
182 ECCO2-Darwin was integrated using a “best guess” set of initial and bound-
183 ary conditions. We will refer to this simulation as “VERSION 1” or “V1”.

184 *3.1. Initial and Boundary Conditions*

185 The ECCO2-Darwin model was initialized in January 2004 with physical
186 initial conditions provided by the adjoint-method-based solution described
187 in Section 2.1. Biogeochemical initial conditions for the spin-up were pro-
188 vided by an eight-year integration of Darwin driven by an earlier ECCO2
189 solution. The ecosystem model of that simulation was that of Dutkiewicz
190 et al. (2009). This earlier ECCO2 simulation did not include carbon chem-
191 istry and had been initialized with phosphate, nitrate, and silicate fields
192 from the World Ocean Atlas (Garcia et al., 2006b), and all other fields from
193 an ECCO-GODAE solution (Dutkiewicz et al., 2009), with the exception of
194 iron fields that were provided from MIT’s Integrated Global System Mod-
195 eling framework (IGSM; Dutkiewicz et al., 2012) in the Arctic, and ECCO-
196 GODAE for the rest of the world. Phyto- and zooplankton biomass were from
197 ECCO-GODAE, equally distributed over all types. The initial conditions for
198 *DIC*, alkalinity, and oxygen were taken from a realization of the Community

199 Climate System Model (CCSM-3) ocean Biogeochemical Elemental Cycle
200 (BEC) model (Blackmon et al., 2001; Lovenduski et al., 2007; Doney et al.,
201 2009) that had been spun up for 600 years to pre-industrial conditions and
202 then continued with historical atmospheric CO₂ for 1765 through 2004.

203 *3.2. Model Spin-Up and Experimental Set-Up*

204 The ECCO2-Darwin model spin-up started January 2004 with two years
205 of identical physical atmospheric boundary conditions provided by the 2004
206 adjoint-method ECCO2 solution described in Section 2.1. The two year spin-
207 up was followed by a “ramp-up” for the years 2004 through 2008. For this
208 period the atmospheric boundary conditions were obtained from the Japan
209 Meteorological Agency and Central Research Institute of Electric Power In-
210 dustry 25-year reanalysis (JRA-25; Onogi et al., 2007).

211 The “V1” ECCO2-Darwin simulation, which is described and evaluated
212 below, used physical boundary conditions from the ECCO2 adjoint solution
213 for the year 2009 and for the first four months of 2010, followed by JRA-25
214 forcing for the remainder of 2010. Surface boundary conditions for dust/iron
215 deposition were provided by the climatology of Mahowald et al. (2006). At-
216 mospheric $p\text{CO}_2$ forcing fields were constructed from spatially variable, daily
217 atmospheric $p\text{CO}_2$ fields from 2009 GEOS-Chem results (Nassar et al., 2010)
218 produced as part of the NASA CMS Flux Pilot Project. The spatial and
219 temporal anomalies of these fields were adjusted globally using the global
220 atmospheric monthly $p\text{CO}_2$ means from NOAA’s Earth System Research
221 Laboratory².

222 *3.3. Results and Evaluation*

223 One of the most striking features of the simulations with ECCO2-Darwin
224 is the high temporal and spatial variability of air-sea CO₂ fluxes. The day-to-
225 day variability in the mid- and high latitudes is dominated by synoptic scale
226 atmospheric systems. An example from this simulation for six consecutive
227 days in January 2009 is shown in Fig.1. The air-sea exchange processes
228 are dominated by wind speed variability (which is parameterized through
229 a quadratic dependence of the air-sea flux on the wind speed, Wanninkhof,
230 1992). While the reflection of atmospheric synoptic activity in air-sea gas

²NOAA’s ESRL data provided through their website at <http://www.esrl.noaa.gov/gmd/ccgg/trends/>

231 exchange fluxes is not surprising, it is worth pointing out that this high
232 variability is lost when using flux climatologies (e.g., Takahashi et al., 2009)
233 to drive atmospheric models.

234 One method to evaluate the quality of our model calculations is to com-
235 pare our globally integrated mean CO₂ exchange to published values de-
236 rived from other ocean models (for instance in a synthesis like: Global Car-
237 bon Project, 2011). There, the global ocean uptake for 2010 is given as
238 $2.4 \pm 0.5 \text{ PgCyr}^{-1}$. Our “VERSION 1” run yields 3.6 PgCyr^{-1} (compare
239 Tab.1). The temporal evolution of this globally integrated flux is shown in
240 Fig.2 for 2009 and 2010. The blue circles represent our “V1” run, the thick
241 black lines monthly mean values from Takahashi et al. (2009), which are
242 referenced to 2000. The annual cycle of global uptake and outgassing can
243 be explained by looking at processes in some key regions. As the processes
244 shaping the time-series are the same for the other model realizations and
245 only differ in magnitudes, we will discuss them later in Section 7.

246 With the overall uptake of the ocean in VERSION 1 being clearly too
247 strong, we changed our experimental set-up. The results for V1 were made
248 publicly available as an intermediate result³.

249 4. Sensitivity Experiments

250 To improve the air-sea CO₂ fluxes from our initial run we performed
251 a suite of sensitivity experiments spanning the years 2009 and 2010. The
252 physical initial conditions were identical for all runs (and the same as those
253 described in Section 3.1). Five runs (CCSM, GLODAP, KS, BLEND, and
254 NOBM) varied in their biogeochemical initial conditions and were spun-up
255 as described in Section 3.1 starting with the year 2004. Additional sensitiv-
256 ity runs varied model parameterizations (runs PISVEL and PICPOC) while
257 using the January 2009 biogeochemical fields of the GLODAP integration as
258 initial conditions.

259 4.1. Run Descriptions

260 The initial conditions that distinguish the sensitivity runs were created
261 by interpolating the data sets described in the following to ECCO2-Darwin’s
262 cube sphere grid. An overview of the parameterizations and initial conditions
263 used in the integrations is given in table 1.

³<http://cmsflux.jpl.nasa.gov/>

264 *CCSM run.* The CCSM run is basically identical to V1. The only difference
265 to V1 lies in the use of two complete years of adjoint forcing for the years
266 2009 and 2010 for the CCSM run. The initial conditions for *DIC*, alkalinity,
267 and oxygen were taken from a realization of the Community Climate Sys-
268 tem Model (CCSM-3) ocean Biogeochemical Elemental Cycle (BEC) model
269 (Lovenduski et al., 2007; Doney et al., 2009). More details can be found in
270 the description of run V1 in Section 3.1.

271 *GLODAP (BASELINE) run.* For the GLODAP run the initial conditions for
272 *DIC* and alkalinity were taken from the Global Ocean Data Analysis Project
273 (GLODAP) annual mean climatology provided by the Carbon Dioxide In-
274 formation Analysis Center (CDIAC; Key et al., 2004). The oxygen values
275 were derived from the World Ocean Atlas (WOA; Garcia et al., 2006a) by
276 taking the January values where available (that is, for the top 1500m) and
277 the annual climatology for the rest of the domain. This model realization
278 will also be referred to as “BASELINE” run.

279 *KS run.* Alkalinity and oxygen initial conditions for the KS (Key & Sabine)
280 run were identical to the ones used in the GLODAP run. For *DIC* the
281 CDIAC data set was blended with an anthropogenic correction using the data
282 set from Sabine et al. (2004). The values for initial conditions for January
283 2009 were calculated according to the method described in Le Quéré et al.
284 (2010).

285 *BLEND run.* For the BLEND run *DIC*, alkalinity and oxygen were blended
286 from the initial conditions of three other runs: the fields north of 40°N were
287 identical to CCSM, between 35°N and 15°N to GLODAP, and south of 10°N
288 to KS. The areas between these regions (from 40°N to 35°N and 15°N to
289 10°N) were linearly interpolated in between the data set. In addition, *DIC*
290 values in Antarctic Bottom Water were increased by 10 μmolkg^{-1} .

291 *NOBM run.* Values for the initial conditions of *DIC* and dissolved organic
292 carbon (*DOC*) were taken from a realization of the NASA Ocean Biogeo-
293 chemical Model (NOBM; Gregg et al., 2003; Gregg and Casey, 2007, 2009)
294 provided by Watson Gregg, NASA Goddard Space Flight Center. As this
295 model does not carry alkalinity and oxygen, these quantities were initialized
296 with the data sets used in the BLEND run.

297 *PISVEL run.* The PISVEL run was designed to identify the dependency of
298 our air-sea CO₂ fluxes to their parameterization. To this end we modified the
299 air-sea gas exchange piston velocity in the formulation of Wanninkhof (1992)
300 from our standard value of 0.337 used in the other runs to the original value
301 of 0.31 used by Wanninkhof (1992). This run was started in 2009 using initial
302 conditions from the BASELINE run.

303 *PICPOC runs.* The PICPOC runs take into account the dependency of air-
304 sea CO₂ fluxes on alkalinity. One big driver of alkalinity changes is the
305 cycling of particulate inorganic carbon (*PIC*), which is formed as calcium
306 carbonate (CaCO₃) in shells in some phytoplankton species and subsequently
307 dissolved at depth. The amount of *PIC* produced by these species relative to
308 particulate organic carbon (*POC*) is the parameter we choose to manipulate
309 for the PICPOC+ and PICPOC- experiments from 0.04 in the BASELINE
310 run to 0.1 and 0.01, respectively. For an overview of the variability of this
311 ratio for a variety of ocean regions see Sarmiento et al. (2002). The PICPOC
312 runs were also started in 2009 using initial conditions from the BASELINE
313 run.

314 *Other runs.* We performed further sensitivity experiments varying the disso-
315 lution rate of *PIC* and vertical tracer diffusion. As these runs yielded little
316 to no effect on air-sea CO₂ fluxes or led to inconclusive results we did not
317 pursue them further.

318 4.2. Results and Evaluation

319 Overall, most of our sensitivity experiments reproduced the spatial and
320 temporal patterns observed in biogeochemical quantities; amplitudes, either
321 globally or with regard to specific regions, were not always well matched. As
322 an illustration, the two top rows of Figure 3 show annual means of surface
323 *DIC* from four of our sensitivity runs for 2009. The bottom left shows the
324 values from the GLODAP (Global Ocean Data Analysis Project; Key et al.,
325 2004) climatology that had been used to initialize our “GLODAP” sensitivity
326 experiment (top left of Fig.3). The differences that can be seen between the
327 climatology and the model runs can be attributed to a variety of causes.
328 First, the initial *DIC* fields of the model runs differed from each other quite
329 substantially and thus led to a variety of patterns and amplitudes while the
330 model runs tried to adjust to them. Second, the GLODAP climatology is
331 based on measurements taken in the 1990s and does not reflect contemporary

332 *DIC* fields. It can therefore not be expected that the observational panel in
333 Fig.3 would match the model results for 2009. Furthermore, the GLODAP
334 *DIC* climatology does not cover the Arctic Ocean, nor several marginal seas
335 represented in our model. For our GLODAP run we therefore created values
336 for these areas by extrapolating from nearest neighbors. The errors that
337 might have been introduced by this method are reflected in the substantial
338 differences between model runs that we see, for instance, in the Arctic Ocean.

339 Monthly mean air-sea CO₂ fluxes from our model runs are compared to
340 each other and the data set by Takahashi et al. (2009) in Fig.4 for July 2009
341 and in Fig.5 for January 2010. The strongest discrepancies between model
342 and observations exist in the Southern Ocean. Measurements are notoriously
343 sparse in this region of the world ocean (especially in winter) and this lack of
344 information is reflected in a climatology like that by Takahashi et al. (2009)
345 (lower left in Figs.4 and 5). In these graphs the coarse spatial resolution
346 of the climatology (5°-by-4°) is clearly distinguishable from the high model
347 resolution (approximately 18 km, plotted here as 0.25°) by the absence of
348 fine scale structure. The monthly means of the Takahashi et al. (2009) data
349 set are referenced to the year 2000, while the model results are shown for
350 July 2009 and January 2010. The global uptake of CO₂ by the oceans is
351 modulated by the increase of atmospheric CO₂ concentrations and natural
352 and anthropogenic climate variability (e.g., Le Quéré et al., 2009). Due
353 to all these factors discrepancies between models and observations are not
354 surprising.

355 In July 2009 the main differences between the model runs in Fig.4 lie in
356 the strength of the outgassing in the equatorial Pacific, the spatial extension
357 of the subtropical outgassing in the Northern hemisphere, and the structure
358 and size of air-sea gas exchange fluxes south of 30°S. For January 2010 (Fig.5)
359 the model runs all share the strong oceanic carbon uptake in the Southern
360 Ocean (contrasted by the weak uptake in the climatology). The differences
361 in equatorial upwelling are similar to the July ones. The model runs disagree
362 on the structure and magnitude of air-sea carbon fluxes north of 40°N.

363 The globally integrated mean ocean uptake for 2010 of our model sen-
364 sitivity runs ranges from 0.62 to 4.18 $PgCyr^{-1}$ (see Tab.1) compared to
365 $2.4\pm 0.5 PgCyr^{-1}$ (Global Carbon Project, 2011). The red and green circles
366 in Fig.2 represent two of our sensitivity runs (GLODAP and NOBM), the
367 blue dots our V1 run, and the thick black lines monthly mean values from
368 Takahashi et al. (2009) (which are referenced to 2000). A further discussion
369 of the spatial patterns and the time-series of air-sea CO₂ fluxes and their

370 causes, as well as an evaluation, will be given in Section 7.

371 5. $p\text{CO}_2$ Data Sets

372 In addition to evaluating our results against climatologies (Key et al.,
373 2004; Takahashi et al., 2009) and global mean values (Global Carbon Project,
374 2011) we also used surface $p\text{CO}_2$ data for 2009 and 2010 from the “Global
375 Surface $p\text{CO}_2$ (LDEO) Database” at the Carbon Dioxide Information Analy-
376 sis Center (Takahashi et al., 2011) to evaluate and improve our model results.

377 The available data for the time period of our model run are very sparse
378 and far from being regularly distributed (Fig.6). We sampled our model
379 sensitivity runs at the times and locations of the measurements. The dis-
380 tribution and shape of the resulting scatter plots (not shown) indicates that
381 there are substantial differences between the data and our model, which can
382 be attributed both to model deficiencies as well as undersampling.

383 The wide spread of our solutions, mainly due to the choice of initial
384 conditions, severely limits the ability to realistically constrain 71% of the
385 atmosphere’s lower boundary. To quantify the data-model mismatch and
386 determine our “best” solution we calculated a cost function (details see Sec-
387 tion 6). The cost is defined as the sum of the quadratic differences between
388 observations and model. Values for the costs per observation (J/N_{OBS}) of
389 the GLODAP run for this initial scenario were the lowest of the runs with
390 variable initial conditions,. We therefore choose this run to be our reference
391 or “BASELINE” run for the following investigations.

392 6. Optimal Linear Combination

393 Recently, two studies have assimilated oceanic $p\text{CO}_2$ data into numerical
394 models: Valsala and Maksyutov (2010) used an offline tracer transport model
395 driven by reanalysis ocean currents, and While et al. (2012) assimilated $p\text{CO}_2$
396 into a biogeochemical ocean general circulation model. Both studies report
397 improvements in representing $p\text{CO}_2$ fields. Here we use $p\text{CO}_2$ measurements
398 to constrain initial conditions and exchange coefficients of a global, eddying
399 biogeochemical ocean model in order to improve air-sea CO_2 flux estimates.

400 6.1. Green’s Function Approach

401 The data assimilation approach used in this study is a least squares
402 method based on computation of model Green’s functions. This approach

403 has previously been used for atmospheric tracer inversions (Enting and Mans-
 404 bridge, 1989; Tans et al., 1990; Bousquet et al., 2000), ocean circulation es-
 405 timates (Stammer and Wunsch, 1996; Menemenlis and Wunsch, 1997; Men-
 406 emenlis et al., 2005a), ocean carbon inversions (Gloor et al., 2003; Mikaloff
 407 Fletcher et al., 2006, 2007), joint ocean-atmosphere carbon dioxide inversions
 408 (Jacobson et al., 2007a,b), and anthropogenic CO₂ sequestration estimates
 409 (Khatiwala et al., 2009).

410 The Green’s function approach involves the computation of Ocean Bio-
 411 geochemistry General Circulation Model (OBGCM) sensitivity experiments
 412 followed by a recipe for constructing a solution that is the best linear com-
 413 bination of these sensitivity experiments. Green’s functions are used to lin-
 414 earize the OBGCM, and discrete inverse theory is used to estimate uncertain
 415 OBGCM parameters. The following discussion is based on the description in
 416 Menemenlis et al. (2005a) and uses, when possible, the notation of Ide et al.
 417 (1997).

Algebraically, the OBGCM can be represented by a set of rules for time-
 stepping a state vector:

$$\mathbf{x}^f(t_{i+1}) = M_i [\mathbf{x}^f(t_i)]. \quad (1)$$

The OBGCM state vector $\mathbf{x}^f(t_i)$ includes the prognostic variables of the bio-
 geochemical model as described in Section 2.2, for instance, *DIC*, alkalinity,
 and oceanic *pCO*₂, on a predefined grid at discrete time t_i . Function M_i rep-
 represents the known OBGCM time-stepping rules. The discretized dynamics
 of the true ocean \mathbf{x}^t are assumed to differ from that of the numerical model
 (1) by a vector of stochastic perturbations:

$$\mathbf{x}^t(t_{i+1}) = M_i [\mathbf{x}^t(t_i), \boldsymbol{\eta}], \quad (2)$$

418 where $\boldsymbol{\eta}$ is a noise process, which is assumed to have zero mean and covariance
 419 matrix \mathbf{Q} . Vector $\boldsymbol{\eta}$ contains a set of uncertain parameters, here initial
 420 conditions, air-sea gas exchange coefficients, and the *PIC/POC* ratio, that
 421 can be used as “controls” for bringing the OBGCM simulation closer to
 422 observations.

The optimization problem aims to estimate parameters $\boldsymbol{\eta}$ given a set of
 observations

$$\mathbf{y}^o = H \begin{bmatrix} \mathbf{x}^t(t_0) \\ \vdots \\ \mathbf{x}^t(t_N) \end{bmatrix} + \boldsymbol{\varepsilon}, \quad (3)$$

423 where vector \mathbf{y}^o represents all available observations during the estimation
 424 period, $t_0 \leq t_i \leq t_N$, H is the measurement function, and residual $\boldsymbol{\varepsilon}$ is a
 425 noise process, which is assumed to have zero mean and covariance matrix
 426 \mathbf{R} . Vector $\boldsymbol{\varepsilon}$ represents measurement errors and all model errors that are not
 427 represented by $\boldsymbol{\eta}$ in (2).

For the Green function approach, Eqs. (2) and (3) are combined, resulting
 in

$$\mathbf{y}^o = G[\boldsymbol{\eta}] + \boldsymbol{\varepsilon}, \quad (4)$$

where G is composed of the observation operator H with the OBGCM func-
 tion M_i . Control parameters $\boldsymbol{\eta}$ are estimated by minimizing a quadratic cost
 function

$$J = \boldsymbol{\eta}^T \mathbf{Q}^{-1} \boldsymbol{\eta} + \boldsymbol{\varepsilon}^T \mathbf{R}^{-1} \boldsymbol{\varepsilon}, \quad (5)$$

where superscript T is the transpose operator. We assume that (4) can
 be linearized about a particular OBGCM trajectory. If the linearization
 assumption holds, (4) simplifies to

$$\mathbf{y}^d = \mathbf{y}^o - G[\mathbf{0}] = \mathbf{G}\boldsymbol{\eta} + \boldsymbol{\varepsilon}, \quad (6)$$

where $\mathbf{0}$ is the null vector, $G[\mathbf{0}]$ is the baseline OBGCM integration sampled
 at the data locations, vector \mathbf{y}^d is the model-data difference, and \mathbf{G} is a
 matrix whose columns are the Green functions of G . Specifically, the j -th
 column of matrix \mathbf{G} is

$$\mathbf{g}_{(j)} = \frac{G[\mathbf{e}_j] - G[\mathbf{0}]}{e_j}, \quad (7)$$

where \mathbf{e}_j is a perturbation vector that is everywhere zero except for element
 j , which is set to e_j . That is, each column of \mathbf{G} can be computed using an
 OBGCM sensitivity experiment. Matrix \mathbf{G} is called the data kernel because
 it relates the data \mathbf{y}^d with model parameters $\boldsymbol{\eta}$. The minimization of (5)
 given (6) is a discrete linear inverse problem with solution

$$\boldsymbol{\eta}^a = \mathbf{P}\mathbf{G}^T\mathbf{R}^{-1}\mathbf{y}^d \quad (8)$$

and uncertainty covariance matrix

$$\mathbf{P} = (\mathbf{Q}^{-1} + \mathbf{G}^T\mathbf{R}^{-1}\mathbf{G})^{-1}. \quad (9)$$

428 This approach has been applied to the initialization and adjustment of the
 429 ECCO2-Darwin model, as is discussed next.

430 *6.2. Solution and Linear Combination*

431 As a first step and proof of concept we started our investigations experi-
432 menting with optimizations using a variety of combinations of the data sets
433 described in Section 5. We present results from one particular realization to
434 illustrate the concept.

435 We used the surface $p\text{CO}_2$ data for 2009 and 2010 from the “Global Sur-
436 face $p\text{CO}_2$ (LDEO) Database” at the Carbon Dioxide Information Analysis
437 Center (Takahashi et al., 2011) as described in Section 5 for the data vector
438 \mathbf{y}° in Eq.3 as a first attempt to constrain our model output. The experiments
439 with this data set alone showed that we could achieve a modest improvement,
440 but that the use of additional data constraints was warranted.

441 The Green’s functions run “GREEN” used two other sets of data con-
442 straints: The global mean air-sea CO_2 flux for 2010 (with a value of 2.4 PgCyr^{-1} ,
443 Global Carbon Project, 2011) and the Takahashi et al. (2009) climatology
444 for the seasonal cycle of $p\text{CO}_2$ (after removing area-weighted monthly means
445 from the original values).

446 *6.3. Set-Up for an Optimized Run*

447 Out of a large number of possible combinations of parameters and runs
448 we choose (after experimenting with a variety of settings) those shown in
449 Tables 1 and 2. The standard errors for the $p\text{CO}_2$ data and climatology were
450 set as the RMS error between data and model realizations. The error for the
451 global mean air-sea CO_2 flux was chosen as 0.01 PgCyr^{-1} .

452 For the optimization run GREEN that we discuss here we used a com-
453 bination of seven sensitivity runs: All five runs that differed in their initial
454 conditions (GLODAP, CCSM, KS, BLEND, and NOBM), the sensitivity
455 study involving changed piston velocity (PISVEL), and one of our runs in-
456 volving changes in the ratio of PIC and POC (PICPOC+). The cost per
457 observation for each of these runs is shown in Tab.2. We choose not to use
458 the results from our other sensitivity runs as the associated changes yielded
459 little to no effect on air-sea CO_2 fluxes.

460 The biogeochemical initial conditions (ICs) for our optimized run were
461 determined from a linear combination of the ICs from those five runs that
462 differed in their initial conditions. The factor for the BASELINE run is the
463 sum of all the factors of the runs that used the BASELINE initial conditions
464 (GLODAP, PISVEL, and PICPOC), the other four factors come directly
465 from the Green’s functions calculation. They are listed for the GREEN run

466 in Tab.2, the parameter values for the gas exchange parameter, and the ratio
467 of PIC to POC can be found in Tab.1.

468 7. VERSION 2: An Optimized Solution

469 The GREEN optimizations yielded substantial cost (that is, data-model
470 mismatch) reductions. While the cost per observation of the sensitivity runs
471 was between 1.04 and 2.18 depending on the run, the optimized solution
472 yielded a cost per observation of 0.82 (Tab.2). A linear combination of the
473 values from the sensitivity runs (applying the multiplication factors directly
474 to the model output values and fields instead of performing the optimized
475 runs) yielded even a slightly lower value. This cost improvement is reflected
476 in the scatter plot of Figure 7. While there is still considerable scatter in the
477 optimized solution (black dots), compared to the VERSION 1 results (red
478 dots) the GREEN solution is closer to the diagonal, as symbolized by the
479 scatter plot density contour lines.

480 The global mean oceanic CO₂ uptake for 2010 that was between 0.62 and
481 4.18 $PgCyr^{-1}$ in the sensitivity runs showed a value of 2.54 $PgCyr^{-1}$ in
482 the optimized run (Tab.1). This is of course not surprising as the error for
483 this quantity had been set to 0.01 $PgCyr^{-1}$ in the optimization calculation
484 posing a strong constraint for the solutions.

485 The corresponding annual cycles of globally integrated air-sea CO₂ fluxes
486 for run GREEN are shown as the large black circles in Fig.2. The optimiza-
487 tion has led to values that are located between the extremes of the sensitivity
488 runs, but show the same overall structure in the seasonal cycle. The regional
489 contributions to the seasonal cycle of globally integrated fluxes in Figure 8
490 help interpret the seasonal cycle of the overall CO₂ uptake and release.

491 Strong uptake in the Southern Ocean in the austral spring and summer
492 dominates the global budget. The annual cycle there is mainly driven by
493 variations in vertical and horizontal transport processes as well as biological
494 production. Temperature differences between summer and winter are not
495 very pronounced (on average about 4°C), hence their influence on solubil-
496 ity and air-sea fluxes is limited. This globally integrated uptake maximum
497 during December and January is intensified by winter-time uptake in the
498 mid-latitudes of the northern hemisphere that is only slightly counteracted
499 by outgassing in the southern mid-latitudes. The equal phasing between the
500 mid-latitudes of the northern hemisphere and the Southern Ocean can also be
501 seen in boreal summer/austral winter when the combined (weak) outgassing

502 of these regions more than compensates for the slight uptake of the southern
503 hemispheric mid-latitudes. This interplay hence explains the seasonal cycles
504 of Fig.2.

505 The spatial maps showing the GREEN optimization for surface *DIC* and
506 the monthly mean $p\text{CO}_2$ are in the lower right plots of Figs.3, 4, and 5, re-
507 spectively. In general, the overall features of the biogeochemical fields look
508 realistic. Unrealistic features of single realizations (for instance, the entire
509 North Atlantic being a carbon sink in the CCSM run in January 2010) have
510 been ameliorated in the optimized runs. The July 2009 CO_2 fluxes are in
511 closer agreement with the Takahashi et al. (2009) climatology than our Jan-
512 uary 2010 results. Features like the strength of the Southern Ocean uptake
513 and the almost complete lack of outgassing in the northernmost Pacific are
514 certainly characteristics of our solutions that need to be explored in more
515 detail.

516 Major differences between the regional time-series of our model run and
517 the Takahashi et al. (2009) climatology in Figure 8 exist in the Equatorial
518 Pacific, the North Atlantic and Pacific, and the Southern Ocean. These are
519 reflected in the comparison of the GREEN run's annual mean CO_2 flux map
520 with the annual mean Takahashi climatology in Figure 9 and will be discussed
521 in the following section.

522 The air-sea fluxes from this GREEN run have been published to the
523 research community as VERSION 2 (v2.0 and v2.1, differing only in the
524 method of interpolation to a lat-lon grid)⁴.

525 8. Summary and conclusions

526 It is difficult to asses how realistic our solutions are, as we don't know
527 the "true" state of the ocean and, in particular, of air-sea CO_2 fluxes. The
528 cost functions can give a rough idea of how much the model-data difference
529 was reduced. Still, we are comparing single measurement points that are
530 subject to local or small scale phenomena and temporal variations (caused,
531 for instance, by eddies) with a global model. The climatologies that we used
532 to initialize or constrain our data with have the problem that they are gridded
533 interpolations from measurements that have been taken over long time spans
534 and often there are large gaps between cruises. Of course, the overall patterns

⁴<http://cmsflux.jpl.nasa.gov/>

535 of these climatologies should be represented in model resolutions, and they
536 are.

537 A different approach to validating the adjusted ECCO2-Darwin simula-
538 tion is to compare our results to other studies. Since other studies have
539 mostly reported annual mean results, we refer to our annual mean air-sea
540 CO₂ flux in Fig.9. The ocean inversion study by Gruber et al. (2009) shows
541 only slight discrepancies between the ocean inversion estimate of uptake in
542 the Southern Ocean (defined as south of 44°S) and the Takahashi et al. (2009)
543 climatology with regard to the overall uptake values, but a very different spa-
544 tial structure. In the climatology CO₂ is taken up near the continent (very
545 weak to neutral in our GREEN run), and released into the atmosphere north
546 of the Antarctic Polar Front (strong outgassing in GREEN). The values in
547 the ocean inversion for the uptake in that area are approximately between
548 0.5 and 3 $molCm^{-2}yr^{-1}$ (nominal for 1995), our model produces values be-
549 tween an outgassing of up to 3 $molCm^{-2}yr^{-1}$ in the Eastern Pacific Sector
550 of the Southern Ocean to an uptake of up to 7 $molCm^{-2}yr^{-1}$ off the coast
551 of Argentina. These overall higher values appear to be more in line with
552 the majority of the OCMIP-2 ocean forward models (Watson and Orr, 2003)
553 that are referred to in Gruber et al. (2009) with a decidedly higher uptake in
554 Southern Ocean. The inverse calculations of Mikaloff Fletcher et al. (2006)
555 find a strongly elevated uptake of anthropogenic CO₂ south of 44°S compared
556 to results from model forward calculations. Other recent model results from
557 the Community Climate System Model (CCSM-3) ocean Biogeochemical El-
558 emental Cycle (BEC) model (Doney et al., 2009) and an isopycnic carbon
559 cycle model (Assmann et al., 2010) show higher overall carbon uptake in
560 the Southern Ocean compared to the Takahashi et al. (2009) climatology.
561 Although spatial patterns and amplitudes vary from model to model, there
562 is general agreement that the climatology underestimates the carbon sink in
563 the Southern Ocean. The carbon uptake of the ECCO2-Darwin solutions in
564 the Southern Ocean is on the high end compared to most other models and
565 to the climatology, causing an overly pronounced amplitude of the seasonal
566 cycle of the globally integrated CO₂ flux.

567 In other areas of the world ocean the ECCO2-Darwin solutions were more
568 consistent with other studies with differences only in magnitudes. The equa-
569 torial outgassing in the Eastern Pacific of run GREEN, for instance, has a
570 shape similar to Doney et al. (2009), the values are closer to those shown
571 by Assmann et al. (2010). The Northern North Pacific in our model does
572 not show the outgassing in the annual mean that is found in the other two

573 models as well as in the climatology.

574 As we constrained our model to achieve a “target” global carbon uptake
575 of about 2.4 to 2.5 $PgCyr^{-1}$, it needs to compensate for the too strong car-
576 bon uptake in the Southern Ocean by weaker uptake or intensified outgassing
577 in other regions. Additional Green’s functions sensitivity experiments would
578 be required to “repair” these regional problems in representing air-sea CO_2
579 fluxes. We are in the process of diagnosing the underlying model physics and
580 biology that cause this overly strong Southern Ocean uptake. Preliminary
581 conclusions are that the model treatment of nutrient fields in combination
582 with the parameterization of biological production is the most likely can-
583 didate for these unrealistic model results. Additional work is underway to
584 improve the model runs for future releases of CO_2 flux products.

585 This proof-of-concept study has shown that the Green’s function method
586 can help adjust OBGCM model parameters and reduce model-data mis-
587 match. The existing ECCO2-Darwin solution remains, however, preliminary
588 in many ways. First, we only used a very small set of observational data
589 to constrain of Green’s function solution. We are in the process of adding
590 data constraints from observed, full-depth profiles profiles of *DIC*, alkalinity,
591 and oxygen. Second, we are experimenting with the utilization of remotely-
592 sensed products like chlorophyll, and other satellite-derived biological or bio-
593 geochemical quantities to vastly expand the number of available constraints.
594 Third, forward-model sensitivity experiments varying additional model pa-
595 rameters are being carried out, which will lead to additional degrees of free-
596 dom for the optimization. Fourth, we are exploring the creation of new sets
597 of biogeochemical initial conditions, which will also expand this parameter
598 space. One specific set of initial conditions that we are exploring is the con-
599 struction of self-consistent data sets of *DIC* alkalinity, and density. We plan
600 to enforce this self-consistency by assuming that the biogeochemical fields
601 correlate with density and by estimating their variation through regression.
602 This method has been used successfully in regional ocean modeling studies
603 (Gruber et al., 2012; Lachkar and Gruber, 2012). Fifth, the model param-
604 eterizations, especially with regard to the choice of phytoplankton species,
605 are being evaluated in greater detail and adjusted to observations. Lastly,
606 a major drawback of the Green’s function approach discussed herein is that
607 computational cost increases linearly with the number of control parameters.
608 Using this approach for detailed regional adjustments would be impractical.
609 For this reason, we are also exploring the application of the adjoint method
610 to the ECCO2-Darwin model. This strategy is similar to that adopted by the

611 ECCO2 project, whereby preliminary model adjustments were carried out us-
612 ing a Green's function approach while the adjoint method was subsequently
613 used to further fine tune the solution. The cost of the adjoint method, while
614 substantial, is largely independent from the number of control parameters.
615 Using the adjoint method, it is possible to simultaneously adjust a large
616 number of degrees of freedom. For example, in the ECCO2 physical-ocean
617 optimizations, of order two billion model parameters have been adjusted us-
618 ing the adjoint method. For ECCO2-Darwin, we plan to adjust the initial
619 and surface biogeochemical boundary conditions in order to fit the observa-
620 tions discussed above. All of the above improvements will lead to gradually
621 more realistic air-sea CO₂ estimates for the NASA CMS project as well as for
622 the underlying physical, biological, and chemical processes that drive these
623 air-sea fluxes.

624 9. Acknowledgments

625 We wish to thank Watson Gregg for providing data from his NOBM runs
626 and Corinne Le Quéré for making available her method to calculate *DIC*
627 initial conditions corrected for the anthropogenic component. This work was
628 made possible by a grant from NASA's CMS Flux Pilot Project.

629 References

- 630 Adcroft, A., Campin, J., Hill, C., Marshall, J., 2004. Implementation of an
631 Atmosphere-Ocean general circulation model on the expanded spherical
632 cube. *Monthly Weather Review* 132, 2845–2863.
- 633 Assmann, K.M., Bentsen, M., Segschneider, J., Heinze, C., 2010. An isopy-
634 cnic ocean carbon cycle model. *Geoscientific Model Development* 3, 143–
635 167.
- 636 Aumont, O., Bopp, L., 2006. Globalizing results from ocean in situ iron
637 fertilization studies. *Global Biogeochemical Cycles* 20, GB2017, 15 pp.
- 638 Baker, D.F., Law, R.M., Gurney, K.R., Rayner, P., Peylin, P., Denning, A.S.,
639 Bousquet, P., Bruhwiler, L., Chen, Y., Ciais, P., Fung, I.Y., Heimann,
640 M., John, J., Maki, T., Maksyutov, S., Masarie, K., Prather, M., Pak,
641 B., Taguchi, S., Zhu, Z., 2006. TransCom 3 inversion intercomparison:
642 Impact of transport model errors on the interannual variability of regional
643 CO₂ fluxes, 1988-2003. *Global Biogeochemical Cycles* 20, GB1002, 17 pp.

- 644 Battle, M., Bender, M.L., Tans, P.P., White, J.W.C., Ellis, J.T., Conway,
645 T., Francey, R.J., 2000. Global carbon sinks and their variability inferred
646 from atmospheric O₂ and δ¹³C. *Science* 287, 2467–2470.
- 647 Blackmon, M., Boville, B., Bryan, F., Dickinson, R., Gent, P., Kiehl, J.,
648 Moritz, R., Randall, D., Shukla, J., Solomon, S., Bonan, G., Doney, S.,
649 Fung, I., Hack, J., Hunke, E., Hurrell, J., Kutzbach, J., Meehl, J., Otto-
650 Bliesner, B., Saravanan, R., Schneider, E.K., Sloan, L., Spall, M., Taylor,
651 K., Tribbia, J., Washington, W., 2001. The Community Climate System
652 Model. *Bull. Am. Meteorol. Soc.* 82, 2357–2376.
- 653 Bousquet, P., Peylin, P., Ciais, P., Le Quéré, C., Friedlingstein, P., Tans,
654 P.P., 2000. Regional changes in carbon dioxide fluxes of land and oceans
655 since 1980. *Science* 290, 1342–1346.
- 656 Buitenhuis, E.T., Rivkin, R.B., Saille, S., Le Quéré, C., 2010. Biogeochem-
657 ical fluxes through microzooplankton. *Global Biogeochemical Cycles* 24,
658 GB4015, 16 pp.
- 659 Conway, T.J., Tans, P.P., Waterman, L.S., Thoning, K.W., Kitzis, D.R.,
660 Masarie, K.A., Zhang, N., 1994. Evidence for interannual variability of
661 the carbon cycle from the National Oceanic and Atmospheric Administra-
662 tion/Climate Monitoring and Diagnostics Laboratory global air sampling
663 network. *J. Geophys. Res.* 99, 22831–22855.
- 664 Doney, S.C., Lima, I., Feely, R.A., Glover, D.M., Lindsay, K., Mahowald, N.,
665 Moore, J.K., Wanninkhof, R., 2009. Mechanisms governing interannual
666 variability in upper-ocean inorganic carbon system and air-sea CO₂ fluxes:
667 Physical climate and atmospheric dust. *Deep Sea Research Part II: Topical*
668 *Studies in Oceanography* 56, 640–655.
- 669 Dutkiewicz, S., Follows, M.J., Bragg, J.G., 2009. Modeling the coupling
670 of ocean ecology and biogeochemistry. *Global Biogeochemical Cycles* 23,
671 GB4017.
- 672 Dutkiewicz, S., Scott, J., Follows, M., 2012. Winners and losers: Ecological
673 and biogeochemical changes in a warming ocean. *Global Biogeochemical*
674 *Cycles*, submitted.
- 675 Enting, I.G., Mansbridge, J.V., 1989. Seasonal sources and sinks of atmo-
676 spheric CO₂ direct inversion of filtered data. *Tellus B* 41B, 111–126.

- 677 Follows, M.J., Dutkiewicz, S., 2011. Modeling diverse communities of marine
678 microbes. *Annual Review of Marine Science* 3, 427–451.
- 679 Follows, M.J., Dutkiewicz, S., Grant, S., Chisholm, S.W., 2007. Emergent
680 biogeography of microbial communities in a model ocean. *Science* 315,
681 1843–1846.
- 682 Follows, M.J., Ito, T., Dutkiewicz, S., 2006. On the solution of the carbonate
683 chemistry system in ocean biogeochemistry models. *Ocean Modelling* 12,
684 290–301.
- 685 Galbraith, E.D., Gnanadesikan, A., Dunne, J.P., Hiscock, M.R., 2010. Re-
686 gional impacts of iron-light colimitation in a global biogeochemical model.
687 *Biogeosciences* 7, 1043–1064.
- 688 Garcia, H.E., Locarnini, R., Boyer, T., Antonov, J., 2006a. World Ocean
689 Atlas 2005, Volume 3: Dissolved Oxygen, Apparent Oxygen Utilization,
690 and Oxygen Saturation. Technical Report NOAA Atlas NESDIS 64. U.S.
691 Government Printing Office. Washington, D.C. 342 pp.
- 692 Garcia, H.E., Locarnini, R., Boyer, T., Antonov, J., 2006b. World Ocean
693 Atlas 2005, Volume 4: Nutrients (phosphate, nitrate, silicate). Techni-
694 cal Report NOAA Atlas NESDIS 64. U.S. Government Printing Office.
695 Washington, D.C. 396 pp.
- 696 Global Carbon Project, 2011. Carbon budget and trends 2010. [http://www.
697 globalcarbonproject.org/carbonbudget](http://www.globalcarbonproject.org/carbonbudget).
- 698 Gloor, M., Gruber, N., Sarmiento, J.L., Sabine, C.L., Feely, R.A.,
699 Rödenbeck, C., 2003. A first estimate of present and pre-industrial air-
700 sea CO₂ fluxes patterns based on ocean interior carbon measurements and
701 models. *Geophys. Res. Lett.* 30, 1010.
- 702 Gregg, W.W., Casey, N., 2007. Modeling coccolithophores in the global
703 oceans. *Deep-Sea Res. II* 54, 447–477.
- 704 Gregg, W.W., Casey, N., 2009. Skill assessment of a spectral ocean-
705 atmosphere radiative model. *Journal of Marine Systems* 76, 49–63.
- 706 Gregg, W.W., Ginoux, P., Schopf, P.S., Casey, N., 2003. Phytoplankton
707 and iron: Validation of a global three-dimensional ocean biogeochemical
708 model. *Deep-Sea Res. II* 50, 3143–3169.

- 709 Gruber, N., Gloor, M., Mikaloff Fletcher, S.E., Doney, S.C., Dutkiewicz, S.,
710 Follows, M.J., Gerber, M., Jacobson, A.R., Joos, F., Lindsay, K., Men-
711 emenlis, D., Mouchet, A., Mller, S.A., Sarmiento, J.L., Takahashi, T.,
712 2009. Oceanic sources, sinks, and transport of atmospheric CO₂. *Global*
713 *Biogeochemical Cycles* 23, GB1005.
- 714 Gruber, N., Hauri, C., Lachkar, Z., Loher, D., Frölicher, T.L., Plattner, G.,
715 2012. Rapid progression of ocean acidification in the california current
716 system. *Science* .
- 717 Gurney, K.R., Law, R.M., Denning, A.S., Rayner, P.J., Baker, D., Bousquet,
718 P., Bruhwiler, L., Chen, Y.H., Ciais, P., Fan, S., Fung, I.Y., Gloor, M.,
719 Heimann, M., Higuchi, K., John, J., Maki, T., Maksyutov, S., Masarie, K.,
720 Peylin, P., Prather, M., Pak, B.C., Randerson, J., Sarmiento, J., Taguchi,
721 S., Takahashi, T., Yuen, C.W., 2002. Towards robust regional estimates of
722 CO₂ sources and sinks using atmospheric transport models. *Nature* 415,
723 626–630.
- 724 Heimbach, P., Menemenlis, D., Losch, M., Campin, J., Hill, C., 2010. On the
725 formulation of sea-ice models. part 2: Lessons from multi-year adjoint sea-
726 ice export sensitivities through the Canadian Arctic Archipelago. *Ocean*
727 *Modelling* 33, 145–158.
- 728 Ide, K., Courtier, P., Ghil, M., Lorenc, A.C., 1997. Unified notation for
729 data assimilation : Operational, sequential and variational. *Journal of the*
730 *Meteorological Society of Japan*. Ser. II 75, 181–189.
- 731 Jacobson, A.R., Mikaloff Fletcher, S.E., Gruber, N., Sarmiento, J.L., Gloor,
732 M., 2007a. A joint atmosphere-ocean inversion for surface fluxes of carbon
733 dioxide: 1. Methods and global-scale fluxes. *Global Biogeochem. Cycles*
734 21, GB1019.
- 735 Jacobson, A.R., Mikaloff Fletcher, S.E., Gruber, N., Sarmiento, J.L., Gloor,
736 M., 2007b. A joint atmosphere-ocean inversion for surface fluxes of carbon
737 dioxide: 2. Regional results. *Global Biogeochem. Cycles* 21, GB1020.
- 738 Keeling, R.F., Piper, S.C., Heimann, M., 1996. Global and hemispheric CO₂
739 sinks deduced from changes in atmospheric oxygen concentration. *Nature*
740 381, 218–221.

- 741 Key, R.M., Kozyr, A., Sabine, C.L., Lee, K., Wanninkhof, R., Bullister,
742 J.L., Feely, R.A., Millero, F.J., Mordy, C., Peng, T., 2004. A global ocean
743 carbon climatology: Results from global data analysis project (GLODAP).
744 Global Biogeochemical Cycles 18, GB4031, 23 pp.
- 745 Khatiwala, S., Primeau, F., Hall, T., 2009. Reconstruction of the history of
746 anthropogenic CO₂ concentrations in the ocean. *Nature* 462, 346–349.
- 747 Kuze, A., Suto, H., Nakajima, M., Hamazaki, T., 2009. Thermal and near
748 infrared sensor for carbon observation fourier-transform spectrometer on
749 the greenhouse gases observing satellite for greenhouse gases monitoring.
750 *Applied Optics* 48, 6716–6733.
- 751 Lachkar, Z., Gruber, N., 2012. Response of biological production and air-
752 sea CO₂ fluxes to upwelling intensification in the California and Canary
753 Current Systems. *Journal of Marine Systems* in press.
- 754 Le Quéré, C., Raupach, M.R., Canadell, J.G., Marland, G., Bopp, L., Ciais,
755 P., Conway, T.J., Doney, S.C., Feely, R.A., Foster, P., Friedlingstein, P.,
756 Gurney, K., Houghton, R.A., House, J.I., Huntingford, C., Levy, P.E.,
757 Lomas, M.R., Majkut, J., Metzl, N., Ometto, J.P., Peters, G.P., Prentice,
758 I.C., Randerson, J.T., Running, S.W., Sarmiento, J.L., Schuster, U., Sitch,
759 S., Takahashi, T., Viovy, N., van der Werf, G.R., Woodward, F.I., 2009.
760 Trends in the sources and sinks of carbon dioxide. *Nature Geoscience* 2,
761 831–836.
- 762 Le Quéré, C., Rödenbeck, C., Buitenhuis, E.T., Conway, T.J., Langenfelds,
763 R., Gomez, A., Labuschagne, C., Ramonet, M., Nakazawa, T., Metzl, N.,
764 Gillett, N., Heimann, M., 2007. Saturation of the Southern Ocean CO₂
765 sink due to recent climate change. *Science* 316, 1735–1738.
- 766 Le Quéré, C., Takahashi, T., Buitenhuis, E.T., Rödenbeck, C., Sutherland,
767 S.C., 2010. Impact of climate change and variability on the global oceanic
768 sink of CO₂. *Global Biogeochemical Cycles* 24, GB4007, 10 pp.
- 769 Lenton, A., Metzl, N., Takahashi, T., Kuchinke, M., Matear, R.J., Roy, T.,
770 Sutherland, S.C., Sweeney, C., Tilbrook, B., 2012. The observed evolu-
771 tion of oceanic pCO₂ and its drivers over the last two decades. *Global*
772 *Biogeochemical Cycles* 26, GB2021, 14 pp.

- 773 Losch, M., Menemenlis, D., Campin, J., Heimbach, P., Hill, C., 2010. On
774 the formulation of sea-ice models. part 1: Effects of different solver imple-
775 mentations and parameterizations. *Ocean Modelling* 33, 129–144.
- 776 Lovenduski, N.S., Gruber, N., Doney, S.C., Lima, I.D., 2007. Enhanced CO₂
777 outgassing in the Southern Ocean from a positive phase of the Southern
778 Annular Mode. *Global Biogeochem. Cycles* 21, GB2026.
- 779 Mahowald, N.M., Yoshioka, M., Collins, W.D., Conley, A.J., Fillmore, D.W.,
780 Coleman, D.B., 2006. Climate response and radiative forcing from min-
781 eral aerosols during the last glacial maximum, pre-industrial, current and
782 doubled-carbon dioxide climates. *Geophysical Research Letters* 33, L20705,
783 4 pp.
- 784 Marshall, J., Adcroft, A., Hill, C., Perelman, L., Heisey, C., 1997a. A finite-
785 volume, incompressible navier stokes model for studies of the ocean on
786 parallel computers. *Journal of Geophysical Research* 102, 5753–5766.
- 787 Marshall, J., Hill, C., Perelman, L., Adcroft, A., 1997b. Hydrostatic, quasi-
788 hydrostatic, and nonhydrostatic ocean modeling. *Journal of Geophysical*
789 *Research* 102, 5733–5752.
- 790 McNeil, B.I., Matear, R.J., Key, R.M., Bullister, J.L., Sarmiento, J.L., 2003.
791 Anthropogenic CO₂ uptake by the ocean based on the global chlorofluoro-
792 carbon data set. *Science* 299, 235–239.
- 793 Menemenlis, D., Campin, J., Heimbach, P., Hill, C., Lee, T., Nguyen, A.,
794 Schodlock, M., Zhang, H., 2008. ECCO2: High resolution global ocean
795 and sea ice data synthesis. *Mercator Ocean Quarterly Newsletter* 31, 13–
796 21.
- 797 Menemenlis, D., Fukumori, I., Lee, T., 2005a. Using green’s functions to
798 calibrate an ocean general circulation model. *Monthly Weather Review*
799 133, 1224–1240.
- 800 Menemenlis, D., Hill, C., Adcroft, A., Campin, J., Cheng, B., Ciotti, B.,
801 Fukumori, I., Heimbach, P., Henze, C., Khl, A., Lee, T., Stammer, D.,
802 Taft, J., Zhang, J., 2005b. NASA supercomputer improves prospects for
803 ocean climate research. *EOS* 86, 89, 96.

- 804 Menemenlis, D., Wunsch, C., 1997. Linearization of an oceanic general cir-
805 culation model for data assimilation and climate studies. *Journal of At-*
806 *mospheric and Oceanic Technology* 14, 1420–1443.
- 807 Mikaloff Fletcher, S.E., Gruber, N., Jacobson, A.R., Doney, S.C., Dutkiewicz,
808 S., Gerber, M., Follows, M., Joos, F., Lindsay, K., Menemenlis, D.,
809 Mouchet, A., Müller, S.A., Sarmiento, J.L., 2006. Inverse estimates of
810 anthropogenic CO₂ uptake, transport, and storage by the ocean. *Global*
811 *Biogeochem. Cycles* 20, GB2002.
- 812 Mikaloff Fletcher, S.E., Gruber, N., Jacobson, A.R., Gloor, M., Doney, S.C.,
813 Dutkiewicz, S., Gerber, M., Follows, M., Joos, F., Lindsay, K., Menemen-
814 lis, D., Mouchet, A., Müller, S.A., Sarmiento, J.L., 2007. Inverse estimates
815 of the oceanic sources and sinks of natural CO₂ and the implied oceanic
816 carbon transport. *Global Biogeochem. Cycles* 21, GB1010.
- 817 Nassar, R., Jones, D.B.A., Suntharalingam, P., Chen, J.M., Andres, R.J.,
818 Wecht, K.J., Yantosca, R.M., Kulawik, S.S., Bowman, K.W., Worden,
819 J.R., Machida, T., Matsueda, H., 2010. Modeling global atmospheric CO₂
820 with improved emission inventories and CO₂ production from the oxida-
821 tion of other carbon species. *Geoscientific Model Development* 3, 689–716.
- 822 Onogi, K., Tsutsui, J., Koide, H., Sakamoto, M., Kobayashi, S., Hat-
823 sushika, H., Matsumoto, T., Yamazaki, N., Kamahori, H., Takahashi, K.,
824 Kadokura, S., Wada, K., Kato, K., Oyama, R., Ose, T., Mannoji, N.,
825 Taira, R., 2007. The JRA-25 reanalysis. *Journal of the Meteorological*
826 *Society of Japan* 85, 369–432.
- 827 Pfeil, B., Olsen, A., Bakker, D., et al., 2012. A uniform, quality controlled,
828 Surface Ocean CO₂ Atlas (SOCAT). submitted to *Earth System Science*
829 *Data* .
- 830 Rödenbeck, C., Houweling, S., Gloor, M., Heimann, M., 2003. CO₂ flux
831 history 1982-2001 inferred from atmospheric data using a global inversion
832 of atmospheric transport. *Atmos. Chem. Phys.* 3, 1919–1964.
- 833 Roy, T., Bopp, L., Gehlen, M., Schneider, B., Cadule, P., Frölicher, T.L.,
834 Segschneider, J., Tjiputra, J., Heinze, C., Joos, F., 2011. Regional impacts
835 of climate change and atmospheric CO₂ on future ocean carbon uptake: A
836 multimodel linear feedback analysis. *Journal of Climate* 24, 2300–2318.

- 837 Sabine, C.L., Feely, R.A., Gruber, N., Key, R.M., Lee, K., Bullister, J.L.,
838 Wanninkhof, R., Wong, C.S., Wallace, D.W.R., Tilbrook, B., Millero, F.J.,
839 Peng, T.H., Kozyr, A., Ono, T., Rios, A.F., 2004. The oceanic sink for
840 anthropogenic CO₂. *Science* 305, 367–371.
- 841 Sarmiento, J.L., Dunne, J., Gnanadesikan, A., Key, R.M., Matsumoto, K.,
842 Slater, R., 2002. A new estimate of the CaCO₃ to organic carbon export
843 ratio. *Global Biogeochemical Cycles* 16, 1107, 12 pp.
- 844 Sarmiento, J.L., Gruber, N., 2006. *Ocean Biogeochemical Dynamics*. Prince-
845 ton University Press.
- 846 Séférian, R., Iudicone, D., Bopp, L., Roy, T., Madec, G., 2012. Water mass
847 analysis of effect of climate change on air-sea CO₂ fluxes: The Southern
848 Ocean. *Journal of Climate* 25, 3894–3908.
- 849 Stammer, D., Wunsch, C., 1996. The determination of the large-scale cir-
850 culation of the Pacific Ocean from satellite altimetry using model Green’s
851 functions. *Journal of Geophysical Research* 101, 18,409–18,432.
- 852 Takahashi, T., Sutherland, S., Kozyr, A., 2011. *Global Ocean Surface Wa-
853 ter Partial Pressure of CO₂ Database: Measurements Performed During
854 1957-2010 (Version 2010)*. Technical Report ORNL/CDIAC-159, NDP-
855 088(V2010). Carbon Dioxide Information Analysis Center, Oak Ridge Na-
856 tional Laboratory, U.S. Department of Energy. Oak Ridge, Tennessee.
- 857 Takahashi, T., Sutherland, S.C., Sweeney, C., Poisson, A., Metzl, N.,
858 Tilbrook, B., Bates, N., Wanninkhof, R., Feely, R.A., Sabine, C., Olaf-
859 sson, J., Nojiri, Y., 2002. Global sea-air CO₂ flux based on climatologi-
860 cal surface ocean pCO₂, and seasonal biological and temperature effects.
861 *Deep-Sea Res. II* 49, 1601–1622.
- 862 Takahashi, T., Sutherland, S.C., Wanninkhof, R., Sweeney, C., Feely, R.A.,
863 Chipman, D.W., Hales, B., Friederich, G., Chavez, F., Sabine, C., Wat-
864 son, A., Bakker, D.C., Schuster, U., Metzl, N., Yoshikawa-Inoue, H., Ishii,
865 M., Midorikawa, T., Nojiri, Y., Krtzinger, A., Steinhoff, T., Hoppema,
866 M., Olafsson, J., Arnarson, T.S., Tilbrook, B., Johannessen, T., Olsen,
867 A., Bellerby, R., Wong, C., Delille, B., Bates, N., de Baar, H.J., 2009.
868 Climatological mean and decadal change in surface ocean pCO₂, and net

- 869 sea-air CO₂ flux over the global oceans. *Deep Sea Research Part II: Topical*
870 *Studies in Oceanography* 56, 554–577.
- 871 Tans, P.P., Fung, I.Y., Takahashi, T., 1990. Observational constraints on the
872 global atmospheric CO₂ budget. *Science* 247, 1431–1438.
- 873 Thomas, H., Prowe, A.E.F., Lima, I.D., Doney, S.C., Wanninkhof, R., Great-
874 batch, R.J., Schuster, U., Corbière, A., 2008. Changes in the North At-
875 lantic Oscillation influence CO₂ uptake in the North Atlantic over the past
876 2 decades. *Global Biogeochem. Cycles* 22, GB4027.
- 877 Toth, Z., Peña, M., 2007. Data assimilation and numerical forecasting with
878 imperfect models: The mapping paradigm. *Physica D: Nonlinear Phenom-*
879 *ena* 230, 146–158.
- 880 Valsala, V., Maksyutov, S., 2010. Simulation and assimilation of global ocean
881 pCO₂ and air-sea CO₂ fluxes using ship observations of surface ocean pCO₂
882 in a simplified biogeochemical offline model. *Tellus B* 62, 821–840.
- 883 Wanninkhof, R., 1992. Relationship between wind speed and gas exchange
884 over the ocean. *J. Geophys. Res.* 97, 7373–7382.
- 885 Watson, A.J., Orr, J.C., 2003. Carbon dioxide fluxes in the global ocean,
886 in: Fasham, M.J.R. (Ed.), *Ocean Biogeochemistry: A JGOFS Synthesis*.
887 Springer-Verlag, Berlin. chapter 5, pp. 123–141.
- 888 While, J., Totterdell, I., Martin, M., 2012. Assimilation of pCO₂ data into a
889 global coupled physical-biogeochemical ocean model. *Journal of Geophys-*
890 *ical Research* 117, C03037, 11 pp.
- 891 Wunsch, C., Heimbach, P., 2007. Practical global oceanic state estimation.
892 *Physica D: Nonlinear Phenomena* 230, 197–208.

Table 1: Initial conditions and parameterizations used in sensitivity and optimized experiments plus air-sea CO_2 fluxes for 2010. **Gas Exchange Parameter:** Air-sea gas exchange is calculated following Wanninkhof (1992): Gas transfer velocity $k = \text{fact } u^2 (\text{Sc}/660)^{-0.5}$, with Sc being the Schmidt number of CO_2 in seawater and fact the numerical value in this table; **CCSM:** values are from a realization of the Community Climate System Model (Blackmon et al., 2001; Lovenduski et al., 2007; Doney et al., 2009) in T62 resolution with historic atmospheric CO_2 forcing; **GLODAP:** Global Ocean Data Analysis Project, Carbon Dioxide Information Analysis Center (Key et al., 2004) with anthropogenic correction of Sabine et al. (2004); values for initial conditions calculated according to method described in Le Quéré et al. (2010); **Blended:** DIC , Alk , and O_2 blended from other runs: North of 40°N from CCSM, between 35°N and 15°N from GLODAP, South of 10°N from KS, with linear interpolation in between data sets from 40°N to 35°N and 15°N to 10°N . In addition, DIC values in Antarctic Bottom Water were increased by $10 \mu\text{mol kg}^{-1}$; **NOBM:** Values taken from a realization of the NASA Ocean Biogeochemical Model (NOBM; Gregg et al., 2003; Gregg and Casey, 2007, 2009) provided by Watson Gregg, NASA Goddard Space Flight Center; **GREEN:** Multiplication factors for all biogeochemical initial conditions: $\text{GREEN} = 0.56404 \cdot \text{GLODAP} + 0.16033 \cdot \text{CCSM} - 0.077899 \cdot \text{KS} + 0.10418 \cdot \text{BLEND} + 0.24935 \cdot \text{NOBM}$.

Run name	Initial Conditions			Gas Exchange Parameter	PIC/POC	Flux 2010 [PgC/yr]	Remarks
	DIC	Alk	O_2				
V1	CCSM	CCSM	CCSM	0.337	0.04	-3.61	Published as version 1.0
GLODAP	GLODAP	GLODAP	WOA 2005	0.337	0.04	-3.63	BASELINE run
CCSM	CCSM	CCSM	CCSM	0.337	0.04	-4.18	
KS	GLODAP, Sabine		WOA 2005	0.337	0.04	-3.21	
BLEND	Blended		Blended	0.337	0.04	-3.87	
NOBM	NOBM		Blended	0.337	0.04	-0.62	DOC IC also from NOBM
PISVEL	BASELINE		BASELINE	0.31	0.04	-3.55	
PICPOC+	BASELINE		BASELINE	0.337	0.1	-3.79	
PICPOC-	BASELINE		BASELINE	0.337	0.01	-3.30	
GREEN	Optimization			0.34822	0.133	-2.54	Published as versions 2.0 and 2.1

Table 2: Costs per observation (J/N_{OBS}) and multiplication factors for initial condition calculation for sensitivity and optimized model realizations. The “Linear Combination” refers to a calculation of cost and fluxes simply based on a linear combination of the factors from the sensitivity runs, calculated without actually performing a run.

Run	GREEN	
name	J/N_{OBS}	Factors
GLODAP	1.2819	0.56404
CCSM	1.9681	0.16033
KS	1.0429	-0.077899
BLEND	1.6594	0.10418
NOBM	2.1856	0.24935
PISVEL	1.2892	
PICPOC+	1.0828	
Lin.Combi.	0.8076	
GREEN	0.8242	

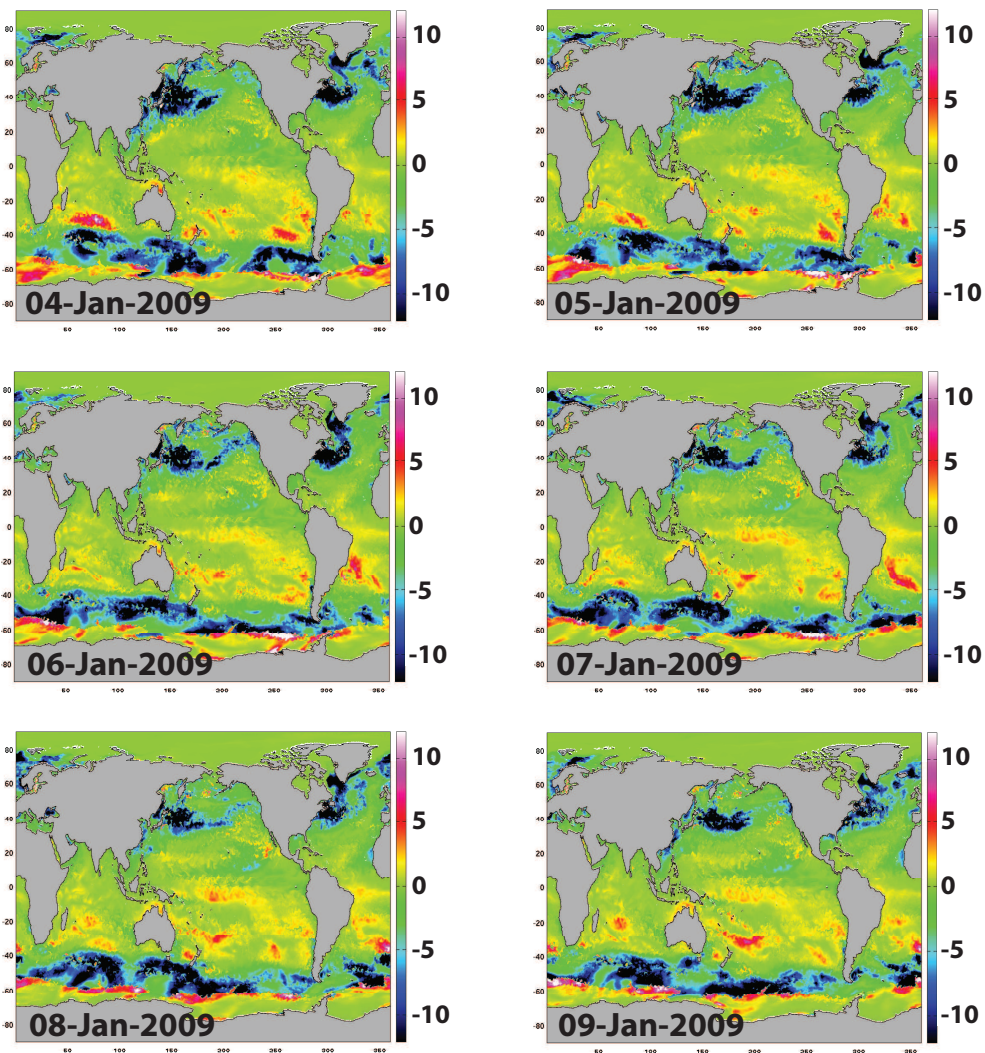


Figure 1: Sequence of 6 daily means of sea-air CO₂ gas fluxes in $\text{molCm}^{-2}\text{yr}^{-1}$ from the “VERSION 1” simulation for January 4–9, 2009. Positive values denote upward fluxes, i.e., outgassing, negative values oceanic uptake. Note the rotating propagation of high and low values from west to east following the paths of atmospheric synoptic systems.

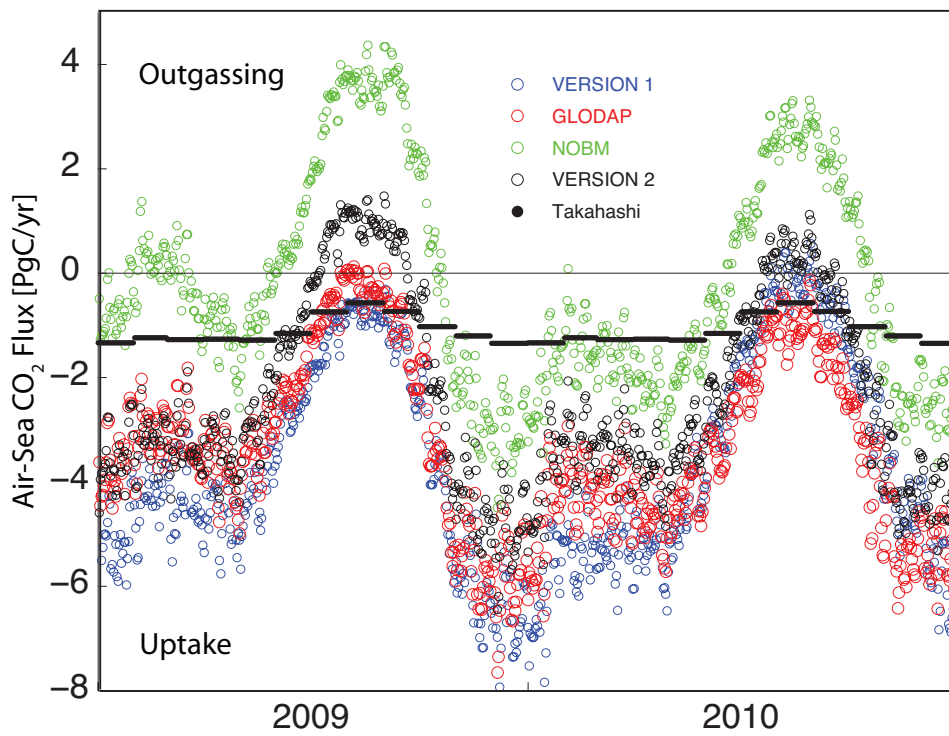


Figure 2: Globally integrated sea-air CO₂ fluxes for 2009 and 2010 in $PgCyr^{-1}$ for four different model realizations: Initial conditions taken from VERSION 1 (blue), NOBM (green), GLODAP (baseline integration, red), GREEN/VERSION 2 (open black circles), and the monthly means derived from Takahashi et al. (2009) (thick black lines).

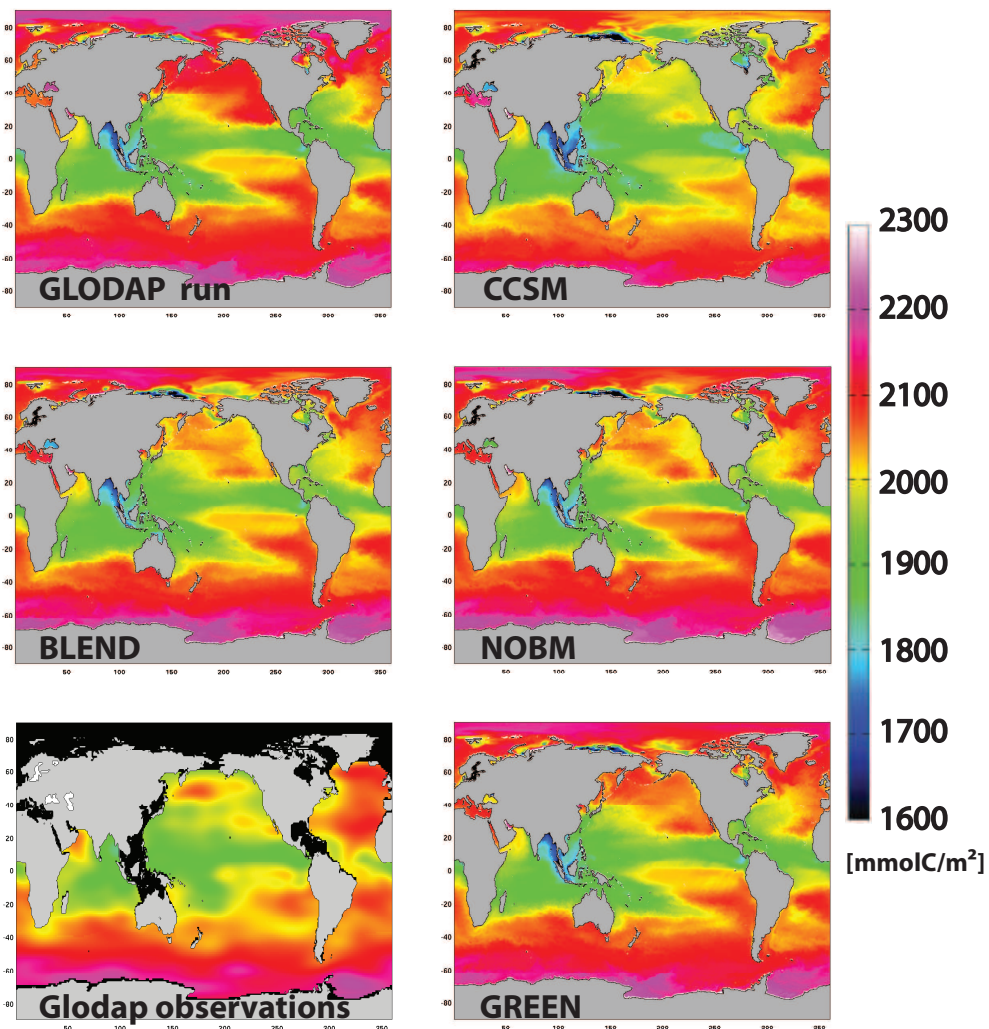


Figure 3: Annual mean of surface dissolved inorganic carbon (DIC) in $mmolCm^{-2}$ for 2009 for model runs GLODAP and CCSM (top), BLEND and NOBM (middle), from the Global Ocean Data Analysis Project data set (Key et al., 2004), and the optimized run GREEN (bottom).

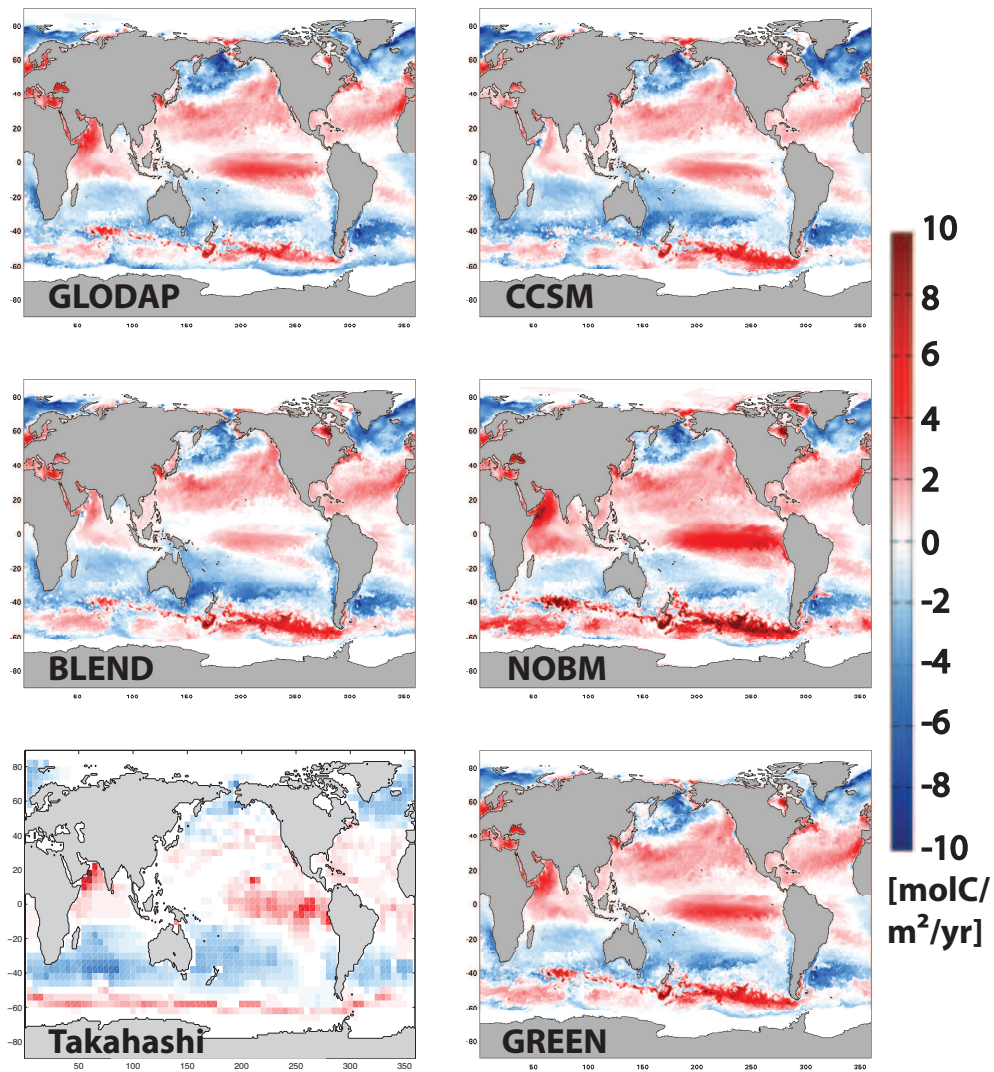


Figure 4: Monthly mean CO₂ gas fluxes in $\text{molCm}^{-2}\text{yr}^{-1}$ for July 2009 for model runs GLODAP and CCSM (top), BLEND and NOBM (middle), from the Takahashi et al. (2009) data set, and the optimized run GREEN (bottom). Positive values (red) are upward.

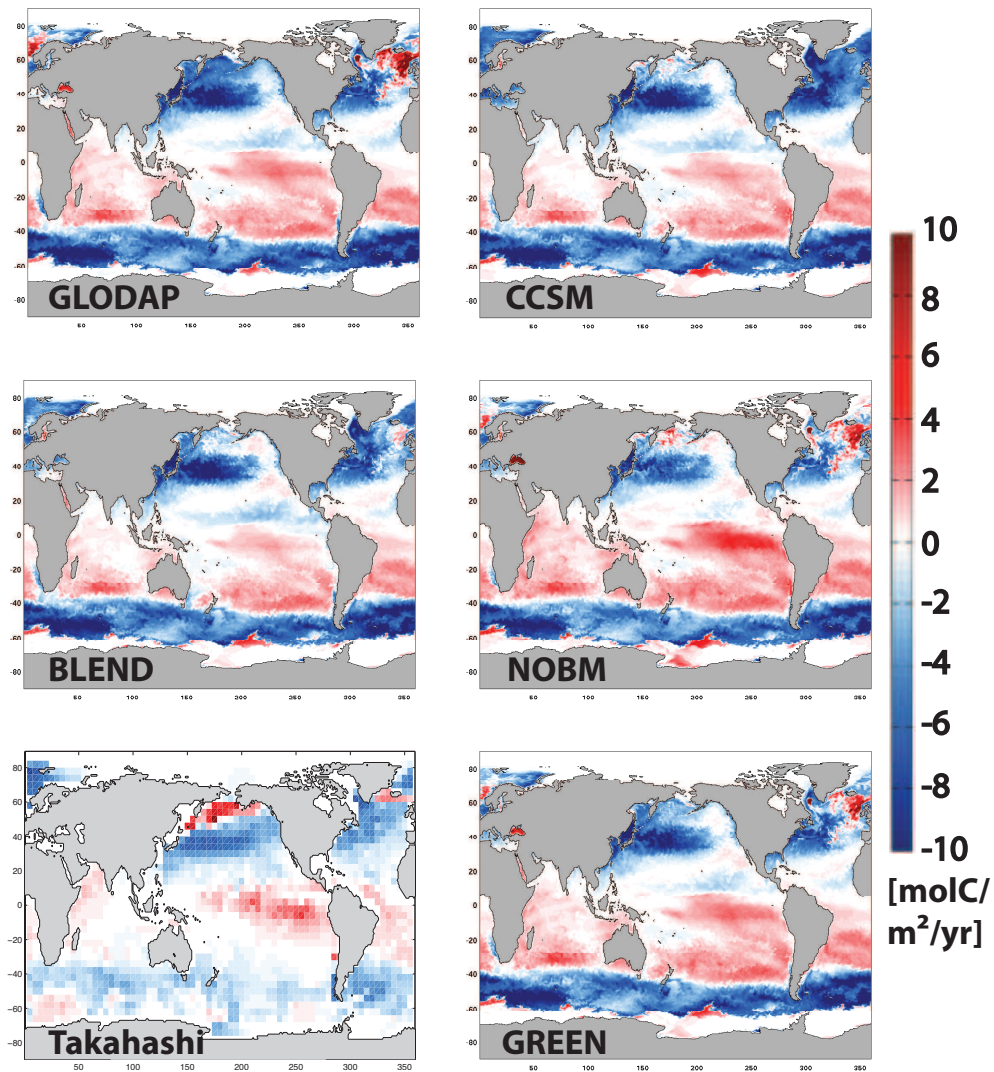


Figure 5: Monthly mean CO₂ gas fluxes in $\text{molCm}^{-2}\text{yr}^{-1}$ for January 2010 for model runs GLODAP and CCSM (top), BLEND and NOBM (middle), from the Takahashi et al. (2009) data set, and the optimized run GREEN (bottom). Positive values (red) are upward.

LDEO_Database_V2010

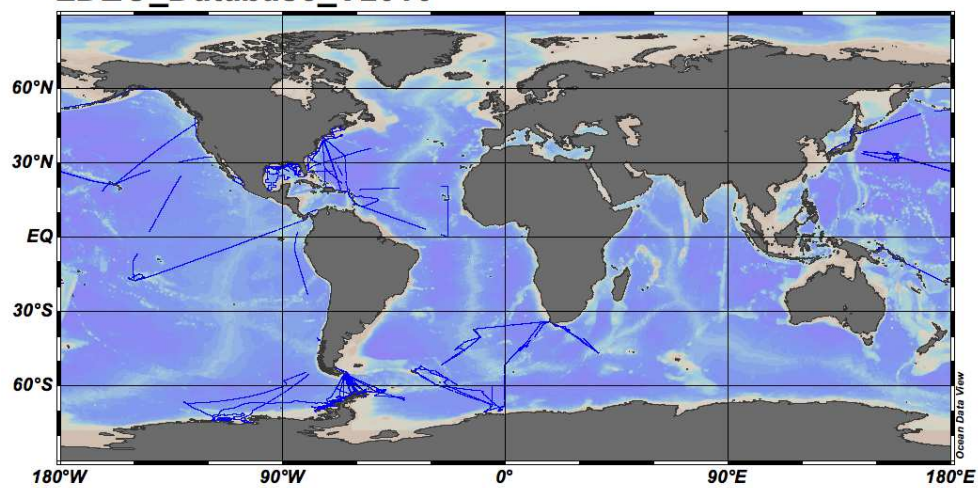


Figure 6: Positions of surface $p\text{CO}_2$ measurements during 2009 and 2010 from the Global Surface $p\text{CO}_2$ database at the Lamont-Doherty Earth Observatory (Takahashi et al., 2011) represented by the blue dots and lines. Graph was created using ODV software (<http://odv.awi.de>).

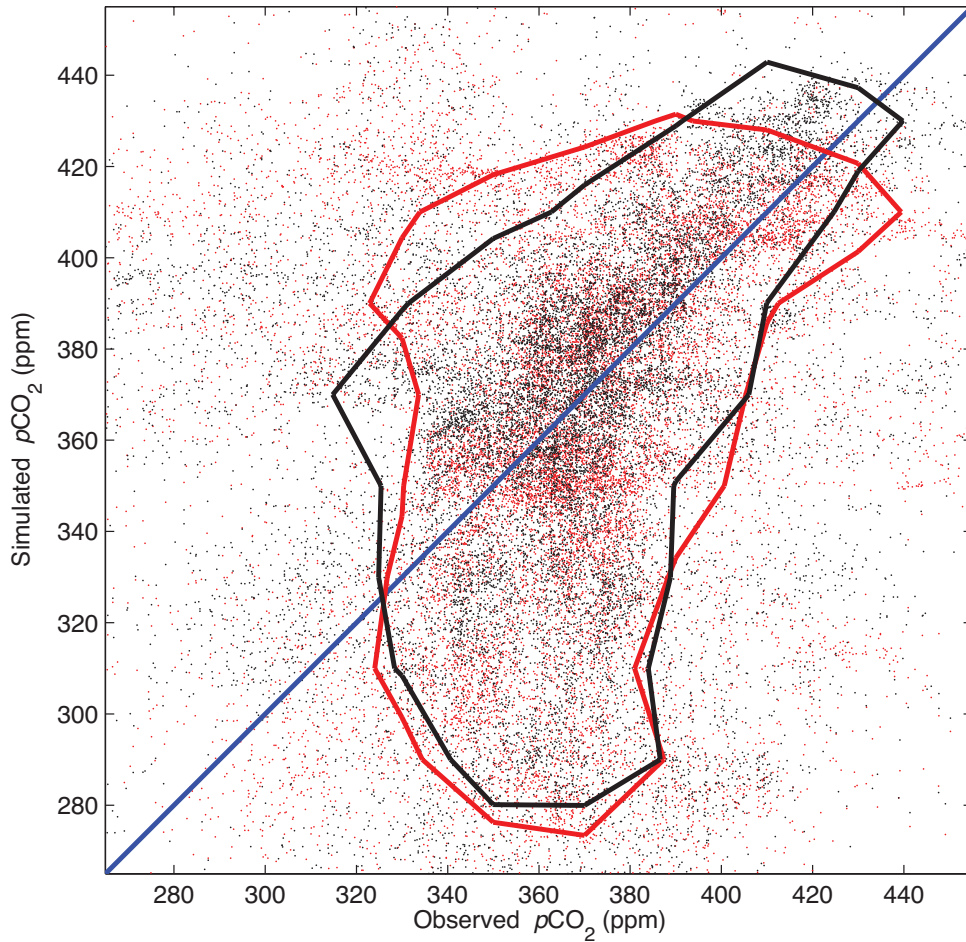


Figure 7: Scatter plots for locations of $p\text{CO}_2$ measurements as depicted in Fig.6, relating model output (vertical axis) to observations (horizontal axis). Red dots and contour line represent VERSION 1, black dots and contour line represent the optimized simulation GREEN/VERSION 2. The contour lines denote regions where scatter plot density is greater than 0.5 points per ppm^2 . The r^2 coefficients for VERSIONS 1 and 2 are 0.05 and 0.09, the slopes are 0.24 and 0.28, respectively.

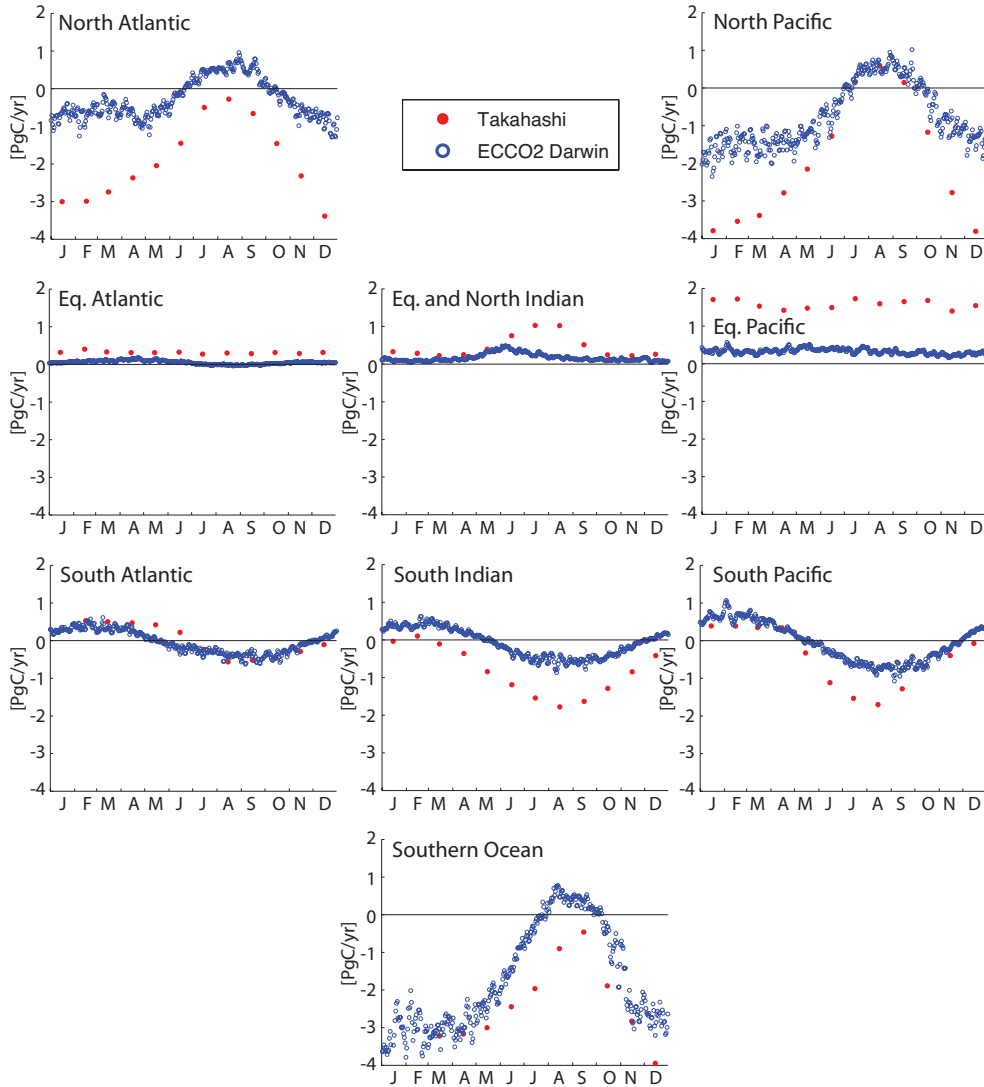


Figure 8: Time-series of regionally integrated sea-air CO_2 fluxes for 2010 from the optimized model run (GREEN/VERSION 2) in PgCyr^{-1} (blue dots) and, for reference, the monthly mean values from the Takahashi et al. (2009) climatology (red dots). Positive values (red) are upward. The black lines in the time-series plots denote “0”, values above this line represent outgassing, below it ocean uptake; the scales are identical for all time-series plots.

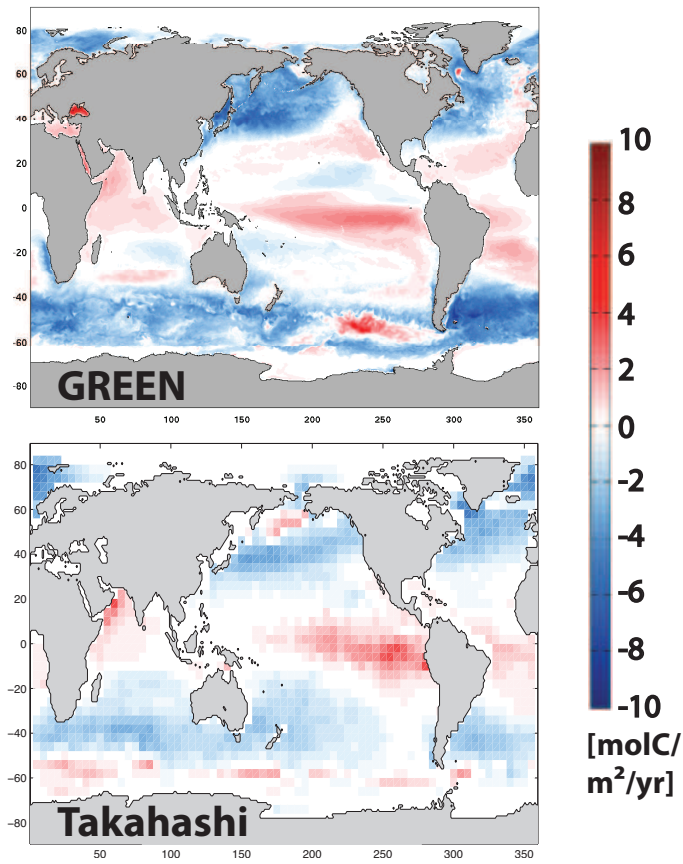


Figure 9: Annual mean CO₂ gas fluxes in $\text{molCm}^{-2}\text{yr}^{-1}$ for 2010 for the optimized model run GREEN (top) and the Takahashi et al. (2009) data set. Positive values (red) are upward.